Hindawi
International Journal of Corrosion
Volume 2018, Article ID 3028693, 13 pages
https://doi.org/10.1155/2018/3028693

Research Article

An Electrochemical Synthesis of Reduced Graphene Oxide/Zinc Nanocomposite Coating through Pulse-Potential Electrodeposition Technique and the Consequent Corrosion Resistance

S. Moshgi Asl,[1] **A. Afshar**,[1] **and Y. Yaghoubinezhad**[2]

[1]*Department of Materials Science and Engineering, Sharif University of Technology, P.O. Box 11365-11155, Tehran, Iran*
[2]*Department of Mechanical and Materials Engineering, Birjand University of Technology, Birjand, Iran*

Correspondence should be addressed to S. Moshgi Asl; s.moshkiasl@gmail.com

Received 24 November 2017; Accepted 21 February 2018; Published 24 April 2018

Academic Editor: Tuan Anh Nguyen

Pulse-potential coelectrodeposition of reduced graphene oxide/zinc (rGO-Zn) nanocomposite coating is directly controlled upon a steel substrate from a one-pot aqueous mixture containing $[GO^{-}/Zn^{2+}]^{\delta+}$ nanoclusters. GO nanosheets are synthesized by modified Hummer's approach while Zn cations are produced in the solution and deposited on GO nanosheets using anodic dissolution technique. Eventually, nanoclusters are reduced to rGO-Zn film through an electrochemical process. Chemical composition, surface morphology, and corrosion resistance of the thin film are characterized. Results show that the corrosion resistance of rGO-Zn coating is approximately 10 times more than the bare steel.

1. Introduction

Although steel finds large applications in various industries because of its superb mechanical strength, it shows poor corrosion resistance due to its thermodynamic instability when exposed to conditions like humidity, high temperature, and acidic solutions [1]. Protection of metals from corrosion is a fundamental issue for many industries. Zinc components are the most widely used coatings for protection of steel against corrosion [2, 3]. The success of using zinc for protection of steel components can be attributed to its low cost, ease of application, and sacrificial nature [2, 4]. By virtue of the fact that, under the same conditions (3.5 wt.% NaCl solution), the potential of zinc is more negative (−1050 mV/SCE) than that of steel (−650 mV/SCE) [3], zinc deposits act as sacrificial anodes and provide cathodic protection of steel [3, 5]. It is known that fine grain size of coatings can effectively improve their corrosion resistance [6]. Accordingly, researchers have made many efforts in order to fine the grain size of zinc coatings and improve their properties [3, 7]. The life time of the Zn coating is however limited due to its rapid dissolution under aggressive environments [8]. Furthermore, prediction of many steel companies about severe deficiency of zinc in 20 to 25 years results in considerable research efforts assigned to enhance the reliability and lifespan of sacrificial Zn coatings [8, 9]. Nowadays, graphene which is a two-dimensional structure of carbon atoms bonded together in a hexagonal honeycomb lattice [1] and is being predicted to have numerous unique characteristics such as chemical inertness [10], exceptional thermal and chemical stability, remarkable flexibility [11], large specific surface area, excellent conductivity, and availability for surface functionalization [1] would be a perfect candidate which can form a passive layer to protect metals from oxidation and corrosion especially in severe marine environment [11, 12]. Graphene coating is believed to be able to suspend the charge transfer at the metal surface without reducing the electrical and optical capabilities of the coated surface [12]. In fact, graphene provides a diffusion barrier for physical separation of the protected metal and reactants [10, 11]. There is growing concern for hybrid

nanocomposites including multiple components, where the components act in harmony to present corrosion resistance and adhesion to steel substrates [9]. Given that zinc metal shows electrochemically active behavior in nanocomposite [13], Hilder et al. [13] studied graphene/zinc nanocomposite. The main challenge of that study was to overcome the stability problems between anionic carboxylate and phenol groups of GO and cationic precursors of Zn^{2+}. So, they kept Zn^{2+} concentration below a critical threshold concentration. Also, He et al. [14] and Punith Kumar et al. [8] experienced graphene/zinc nanocomposite through different procedures.

In the present study an attempt was made to prepare an aqueous suspension of $[GO^{-}/Zn^{2+}]^{\delta+}$ nanoclusters with dimensions of less than 25 nm. In the next step, a cathodic pulse (potential control) electrodeposition was applied to the synthesis of rGO-Zn nanocomposite film on steel. Pulse electrodeposition (PED) has been found to be an effective technique for controlling the electro-crystallization process to produce unique structures with improved properties compared to coatings obtained by direct current (dc) [2, 4]. This method produces a higher instantaneous current density during deposition that results in an increased nucleation rate leading to the formation of a fine-grained and more homogenous surface appearance for coating [3]. The corrosion resistance of coating was investigated by means of polarization and electrochemical impedance spectroscopy (EIS) techniques.

2. Experiment

2.1. Reagents and Materials. Graphite powder (fine and extra pure), $NaNO_3$, $KMnO_4$, H_2SO_4 (98 wt./wt.%), H_2O_2 (30 wt./wt.%), HCl (37 wt./wt.%), Cetrimonium bromide (CTAB), NaCl, and KCl salts were all obtained from Merck company (Germany) and were used as received. Pure zinc sheets (purity 99.99%) were taken from Khalessazan Company (Zanjan, Iran). Water was doubly distilled before use.

2.2. GO Synthesis. GO nanosheets were produced by modification of Hummers Jr. and Offeman's method [15]. The graphite oxide was produced by stirring 10 g graphite powder and 7 g sodium nitrate with 700 mL sulfuric acid (98 wt./wt.%) in an ice-water bath. The solution was stirred and 45 g potassium permanganate was slowly added to the suspension and stirring continued for 2 hours. Then the mixture solution was stirred for an additional 3 days at room temperature. Afterward, 1400 mL of sulfuric acid (3 wt.%) was added to the solution and the temperature was controlled to be about 97°C. The mixture solution was maintained at this temperature and stirred for 2 hours. After that, the temperature got reduced to 55°C and 15 mL of hydrogen peroxide (30 wt.%) was added to the solution to terminate the oxidation reaction. Following that, the solution was stirred at room temperature for about 2 hours. The resultant solution was overnighted and carefully decanted (The bottom sediment was discarded). To remove the impurities, the solution was purified by 25 times completion of the following procedures: centrifugation for 30 min at 4500 rpm, removal of the solution, washing the remaining solid with 200 ml of an aqueous solution (sulfuric acid 3 wt.%, hydrogen peroxide 0.5 wt.%), and sonicating (30 min in the first step and 15 min in the other steps). These procedures were repeated by three times of using HCl (3 wt.%) and three times by H_2O. At the last stage, the resultant material was dried at 70°C to obtain GO powder [16].

2.3. Preparation of $[GO/Zn^{2+}]^{\delta+}$ Nanoclusters in Aqueous Solution. Zinc cations were produced by anodic dissolution method [17] using a three-electrode cell in which a zinc plate (purity 99.99%) with a surface of $1 \times 1\,cm^2$ as a working electrode, a saturated calomel electrode as a reference electrode, and a platinum (Pt) plate as a counter electrode were used. GO was completely dispersed in doubly distilled water. The prepared GO solution with a concentration of 0.15 mg/ml was used as electrolyte (pH = 3.3). Deoxygenation of the electrolyte was carried out for 45 min by argon gas at 400 psi. Then, plastic covers (with some small pores for gas outlet) were placed on air entry ports of the cell and the amount of gas blowing was dropped to a few bubbles per minute. In the next step, cyclic voltammetry (CV) in the potential range of −0.6 to 2.0 V at a scan rate of 30 mV/s was applied to 80 cycles to produce zinc cations. The following mechanism is suggested for the formation of the $[GO^{-}/Zn^{2+}]^{\delta+}$ nanoclusters: depending on pH values in aqueous solution, various Zn species are present in the form of Zn^{2+}, $Zn(OH)^{+}$, $Zn(OH)_2{}^{0}$, $Zn(OH)_3{}^{-}$, and $Zn(OH)_4{}^{2-}$. At pH < 7.0, the predominant species of Zn is Zn^{2+} [18]. The electrostatic attraction between positive zinc ions and negative surface of GO nanosheets (probably, anionic through deprotonation of phenol and carboxylic acid groups) offers a driving force for the movement of Zn cations through the solution and anchoring on GO nanosheets. Due to the electrostatic equilibrium between GO nanosheets and adsorbed Zn cations, $[GO^{-}/Zn^{2+}]^{\delta+}$ nanoclusters are formed in the medium. Zeta potential was carried out using a Zetasizer (ZEN3600, Malvern Company) and the resultant zeta potential was +11.8 mV.

A schematic representation of the proposed mechanism is illustrated in Figure 1. To determine the Zn ions concentration, atomic absorption spectroscopy (AAS) was used. The average concentration of Zn cations reported around 83 ppm (pH = 6.8).

2.3.1. Stabilization of $[GO^{-}/Zn^{2+}]^{\delta+}$ Nanoclusters Suspension. The obtained suspension was unstable and precipitation occurred after a short time (Figure 2(a)). So, 15 mg of CTAB—as a cationic surfactant—was added to stabilize 30 ml of the $[GO^{-}/Zn^{2+}]^{\delta+}$ nanoclusters suspension with a weight ratio of GO/Zn^{2+} = 1.55 mg/mg (Figure 2(b)). The reason for using a cationic surfactant for stabilization is application of negative potential to the substrate during the pulse electrodeposition procedure. Because, in case of iron or steel, anodic or chemical oxidation is accompanied by the dissolution of the metal and the active iron reacts to give iron oxides. As a rule, iron oxides, which are bulky and hygroscopic, do not adhere to the underlying material and the adhesion of the coating is the most critical aspect of the coating-substrate system. The measured zeta potential was +46.3 mV.

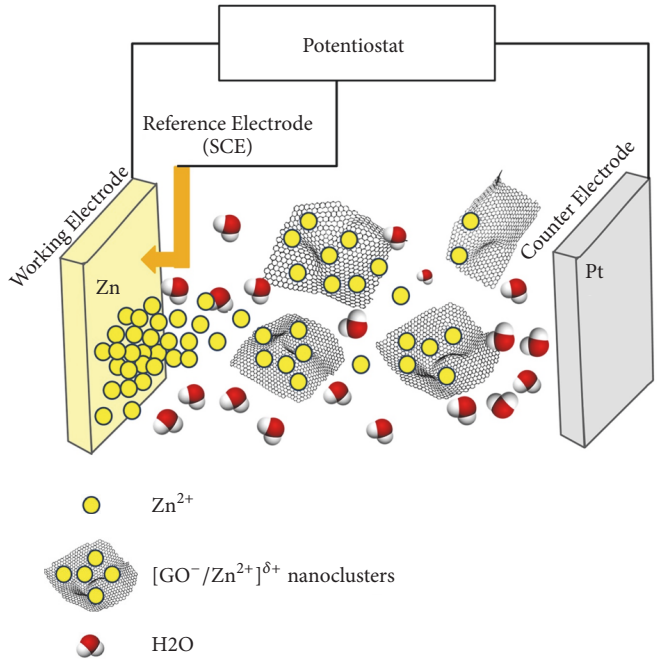

Figure 1: Schematic representation for preparation of $[GO^-/Zn^{2+}]^{\delta+}$ nanoclusters aqueous suspension.

Table 1: Values of pulse electrodeposition (potential control) parameters used for rGO-Zn coating.

Number	Parameter	Value
1	CV cycle	80
2	Duty cycle%	20
3	Frequency (Hz)	140
4	Coating time (min)	20
5	Potential (V/SCE)	−1.35

2.3.2. Investigation of the Electrical Conductivity of the Suspension. The electrical conductivity of the resulting suspension was studied. Conductivity was measured using a conductivity meter and the value was 126.2 $\mu S \cdot cm^{-1}$. The low electrical conductivity could make it difficult for the electrochemical deposition. Thus, 0.1 ml HCl (10 v/v%) was added to the 30 ml of the suspension to increase the conductivity up to 4.5 $mS \cdot cm^{-1}$. Subsequently, pH was reduced to 1.8.

2.4. Electrochemical Procedure

2.4.1. Electrode Preparation. All steel substrates with surface of 1 × 1 cm^2 were mechanically polished with wet silicon carbide (SiC) abrasive papers of P320 to P3000. Then, they were polished with alumina powder of 0.3 micron. Finally, the surfaces of the samples were cleaned using distilled water and degreased by ethanol.

2.4.2. Pulse Electrodeposition Procedure. A constant-potential pulse electrodeposition was carried out using a multichannel Autolab and controlled using Nova 1.8 software.

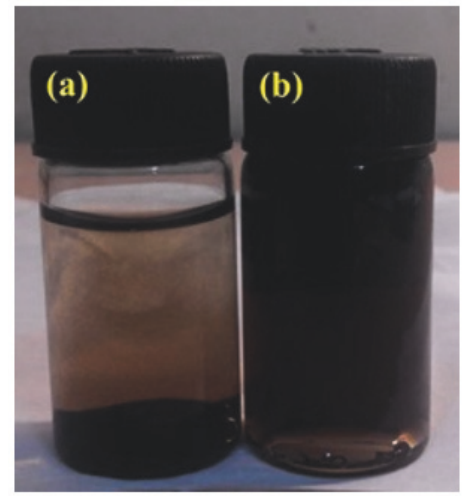

Figure 2: (a) Unstable suspension of $[GO^-/Zn^{2+}]^{\delta+}$ nanoclusters (zeta potential = 11.8 mV); (b) CTAB-stabilized suspension of $[GO^-/Zn^{2+}]^{\delta+}$ nanoclusters (zeta potential = 46.3 mV).

A three-electrode cell system was used consisting of a prepared low carbon steel with a surface of 1 × 1 cm^2 as working electrode, a saturated calomel electrode as reference electrode, and a platinum (Pt) plate as a counter electrode. 30 ml of stable suspension of $[GO^-/Zn^{2+}]^{\delta+}$ was used as electrolyte. A schematic shape of the applied cathodic pulses and parameter values are illustrated in Figure 3 and Table 1, respectively. Considering previous studies [13, 19], reduction potential of −1.35 V was applied. The potential-on time (t_{on})

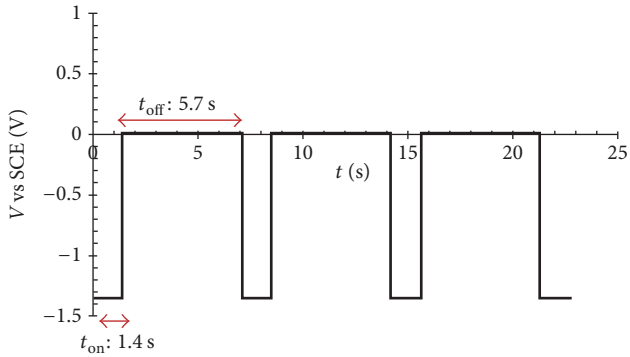

Figure 3: Schematic shape of the applied cathodic pulses during electrodeposition of rGO-Zn nanocomposite (t_{on} = 1.4 ms, t_{off} = 5.7 ms, and D = 20%).

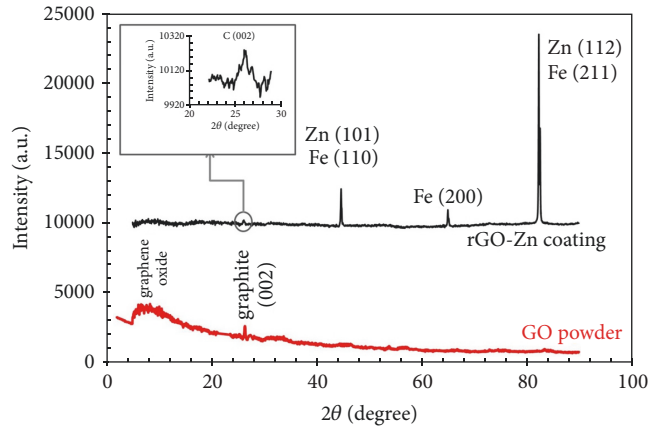

Figure 4: XRD curves of synthesized GO powder according to modified Hummer's method and rGO-Zn coating produced by pulse-potential electrodeposition method.

and the potential-off time (t_{off}) were optimized and kept at 1.4 and 5.7 ms, respectively. This optimization was carried out through a series of electrodeposition experiments in which t_{on} was varied from 0.5 to 5 ms and t_{off} from 5 to 15 ms at constant potential (−1.35 V/SCE). Therefore, duty cycle (D) and frequency (f) that are mathematical quantities achieved from pulse parameters were calculated using the following equations [20]. Furthermore, the desirable coating time to deposit and reduce $[GO^{-}/Zn^{2+}]^{\delta+}$ nanoclusters to rGO-Zn was basically chosen since the fluctuations of current density at the applied potential of −1.35 V/SCE were not significant

$$D = \left[\frac{t_{on}}{(t_{on} + t_{off})}\right] \times 100,$$
$$f = \frac{1}{(t_{on} + t_{off})}. \quad (1)$$

2.5. Characterization. X-ray diffraction (XRD) measurements were carried out using an X-ray diffractometer (STOE-64295) under the Cu-K_α radiation. Data was collected at 2θ from ≈5° to 70° with a step width of 0.039. Diffraction results were analyzed by x'Pert HighScore software. Raman spectra were obtained by the use of micro Raman microscope (BRUKER-SENTERRA, Germany) using a laser with the power of 785 nm within the range of 200–3500 cm^{-1}. Fourier transform infrared (FT-IR) spectroscopy was measured by a spectrometer manufactured by PERKIN-ELMER Company (RXI model) in the range of 4000 to 400 cm^{-1} (in the ATR mode). X-ray photoelectron spectroscopy (XPS) was carried out with a spectrometer (PERKIN-ELMER/PHI Secsa 5000 model) using an X-ray source (with Al target and 1486.6 eV energy and Mg target and 1253.6 eV energy) and a CHA analyzer in the binding energy range of 0–1200 eV. Also, for depth profiling in XPS study, Ar^{+} ions of 1 keV energy and a sputter interval of 3 s were used. The topology and surface roughness of the coating were investigated by atomic force microscopy (AFM). AFM images were obtained by Dualscop C-26 (E50-95 series). The morphology of the GO-Zn film was characterized by field emission scanning electron microscopy (MIRA3-XMU). Coating thickness was measured using the micrographs of the cross section and particle distribution analysis was conducted by distribution map of elements. Before FE-SEM measurements, the surfaces of the samples were covered with a thin layer of gold. The electrochemical properties of coatings were analyzed by polarization test using an Autolab (PGSTAT 302 N) with Nova 1.8 software. A three-electrode cell was used for electrochemical measurement which consists of coated substrate, platinum sheet, and saturated calomel electrode (SCE) as working electrode, counter electrode, and reference electrode, respectively, and 3.5 wt.% NaCl solution was used as corrosive electrolyte. The polarization curves were plotted by sweeping the applied potential from −0.2 to +0.4 V with respect to open circuit potential (OCP) at a scan rate of 1 mV/s on 1 cm^2 working electrode after immersion for 1 hour. The experiments were repeated 2 times to ensure the reproducibility of the results. Further, electrochemical impedance spectroscopy (EIS) test was carried out for corrosion study in 0.1 M KCl electrolyte using EG&G (273 A) with a three-electrode cell. The EIS tests were performed in the frequency range of 10^{-3} to 10^{5} Hz with ac amplitude of 5 mV at OCP to obtain Nyquist plots. Test started when the difference in potential variation for two consecutive points of OCP reached to less than 1 mV. The average time to reach to stable state was about 30 minutes. To ensure repeatability of data, experiments were repeated 2 times. Then, simulation and equivalent electrical circuits were determined using Zsim 4.3 software.

3. Results and Discussion

3.1. Chemical Composition

3.1.1. Characterization by XRD. Figure 4 provides the XRD pattern of GO powder and rGO-Zn film produced by PED. The pattern of GO shows a diffraction peak at 2θ = 10°, corresponding to an interlayer distance of 0.73 nm. The appearance of peak at 10° confirms the formation of GO nanosheets, according to the patterns obtained in previous researches [21]. Moreover, the large interlayer distance of GO nanosheets (0.73 nm) in comparison with graphite interlayer

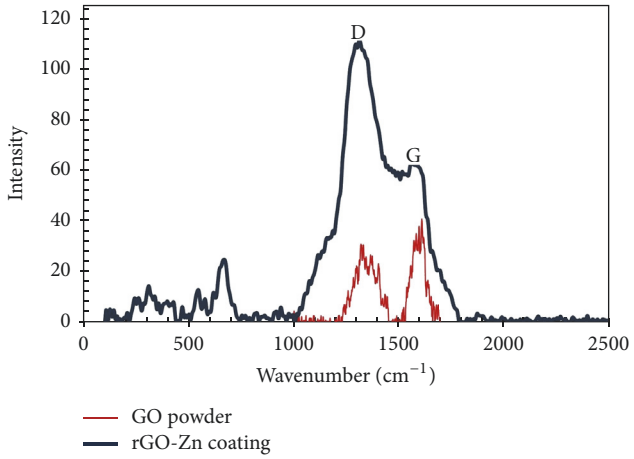

Figure 5: Raman spectra of the GO powder and rGO-Zn coating synthesized by pulse-potential electrodeposition approach.

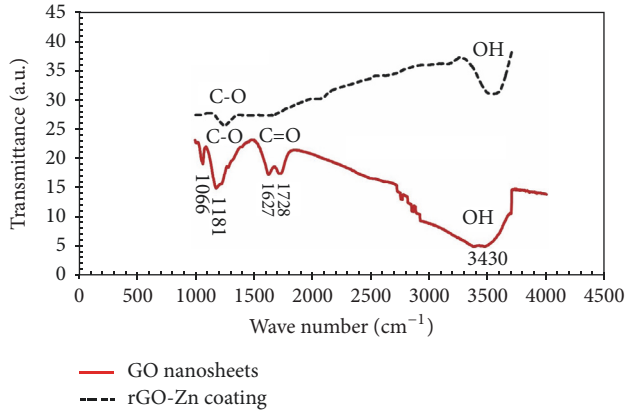

Figure 6: FT-IR spectra of synthesized GO powder and rGO-Zn coating produced by pulse-potential electrodeposition method.

spacing (0.34 nm) [22, 23] demonstrates the presence of oxygen-containing functional groups on GO basal planes [24]. Also, a weak diffraction peak is observed at 26.3° due to diffraction of (002) planes of remaining graphite during the purification of graphene oxide.

The pattern of rGO-Zn coating in Figure 4 shows two peaks at 43.4° and 82.3°. These peaks are related to diffraction of (101) and (112) planes of zinc particles, overlapped with diffraction peaks of (110) and (211) planes of steel substrate, respectively. This result can be attributed to low thickness of rGO-Zn coating. Although there is a very small peak at 26.1° that can be attributed to diffraction of (002) carbon planes [25], the characteristic peak of graphene nanosheets (reduced from GO during electrochemical reduction) was not observed in rGO-Zn pattern like most other similar studies [14, 22, 26]. Low thickness of the formed graphene sheets can be a reason for the lack of characteristic peak for graphene in the diffraction pattern of coating. We can also outline other reasons like low thickness of coating and higher concentration of zinc compared to graphene that elevates the intensity of other peaks in diffraction pattern which make it difficult to observe other lower-intensity peaks. Hence, to ensure about the formation of graphene nanosheets in composite coating, Raman spectroscopy test was conducted on rGO-Zn coating.

3.1.2. Evaluation of rGO-Zn Film by Raman Spectroscopy. Figure 5 represents Raman spectra of synthesized GO nanosheets along with rGO-Zn coating. The spectrum of GO includes D band at 1343 cm^{-1} which is consistent with reported results [27, 28]. The D band appears due to irregularities in the atomic arrangements or effects of graphene edges and microwaves [29].

When layers are perfect, D band does not appear [30]. The second peak in 1595 cm^{-1} is for G band that Ramesha and Sampath reported 1610 cm^{-1} for G band [28]. The origin of G band is plate vibrations of sp^2 carbon atoms [10, 31]. G band of graphite appears at 1583 cm^{-1} and the shift of G band in graphene oxide toward larger amounts can result from G and D′ (due to activation of defects) bands overlapping and decline in layers numbers [28]. According to the Raman spectrum of GO and numerous structural defects which result in high reactivity of synthesized graphene oxide, possibility of rGO-Zn composite formation can be explained. It can be observed that the D (1343 cm^{-1}) and G (1595 cm^{-1}) bands of GO are, respectively, shifted to 1313 cm^{-1} and 1562 cm^{-1} in rGO-Zn coating. The shift is attributed to the recovery of hexagonal network of carbon atoms having defects. Comparing the two spectra, it is clearly seen that the intensity of the G band is higher than the D band in the GO spectrum while, in the nanocomposite, the intensity of the bands is reversed. Change of the intensity ratio of two bands could be due to the increasing defects in reduced graphene oxide [14, 28] and shows that more new graphitic domains have been created and the number of sp^2 areas has increased [32]. In other words, the average size of sp^2 areas is reduced during the reduction of graphene oxide [33]. It has been proved that the intensity ratio of these peaks indicates defect density in carbon materials [19, 34]. Also, I_G/I_D is used to determine the number of graphene layers. Typically, $I_G/I_D < 0.8$ means that the number of layers is less than 6 [35]. In this work, the intensity ratio of composite coating (rGO-Zn) is 0.58 which proves graphene layers in composite are less than 6. While this ratio is equal to 1.33 for GO. Accordingly, the number of layers has been reduced during the pulse-potential electrochemical reduction.

3.1.3. Assessment of the rGO-Zn Nanocomposite by FT-IR. Figure 6 shows FT-IR spectrum of GO sheets. For oxygen-containing functional groups, the main peak is at the wave number of 3430 cm^{-1} due to stretching vibrations of OH groups [36]. The peaks at 1728 cm^{-1} and 1627 cm^{-1} are attributed to C=O bond vibrations in carboxylic and carbonyl moiety functional groups which is in good agreement with the results of Rattana et al. [27]. Two peaks at 1066 cm^{-1} and 1181 cm^{-1} are caused by stretching vibrations of C-O bond [27, 36]. Overall, FT-IR spectrum of GO confirms existence of various active oxygen-containing groups (carboxylic groups at the edges and hydroxyl groups on the base plates) on the internal and external surfaces of GO nanosheets which

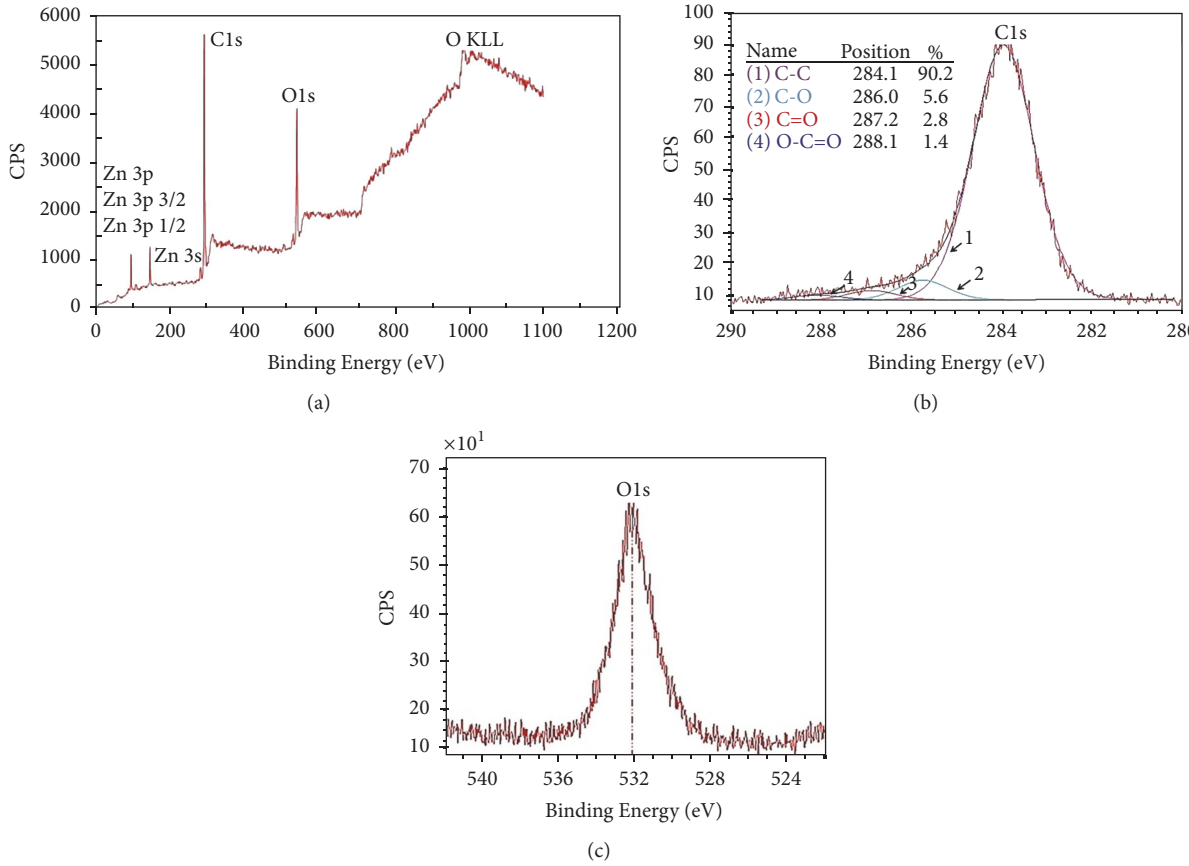

Figure 7: XPS spectra of rGO-Zn coating produced by pulse-potential electrodeposition method (a) survey spectrum of the coating with three major peaks of carbon, oxygen, and zinc. XPS high resolution survey of (b) C1s and (c) O1s peaks of coating.

can affect the surface polarity and further change the surface charges [24]. FT-IR spectrum of rGO-Zn coating is also illustrated in Figure 6. It is observed that, after pulse- potential electrochemical reduction, the peak related to O-H stretching vibrations has become small and narrow and absorption peaks of C=O bond vibrations have almost completely eliminated. In addition, the existing peak at 1181 cm^{-1} due to stretching vibrations of C-O and epoxy groups is very small and insignificant. This result shows that reduction of graphene oxide to graphene nanosheets by electrochemical pulse method is well done and oxygen-containing groups have been removed from carbon planes with good approximation.

3.1.4. XPS Analysis of the rGO-Zn Coating. XPS is a surface analysis technique used to study the chemical environment of atoms [32]. Figure 7(a) shows the survey spectrum of coating. According to this spectrum, surface of coating is composed of carbon, oxygen, and zinc atoms. To assess the relative amount of oxidation, the ratio of C/O is not used, because full reduction of graphene oxide is very difficult and this ratio is not reliable; thus C1s peak is used [36]. The spectra were calibrated according to C-C peak position at 284 ± 0.2 eV. Resolution of the spectrometer does not provide a separate analysis of C-C and C=C peaks. So they were considered as a single peak and compared with the peaks attributed to carbon bonding with other functional groups. Figure 7(b) shows high resolution survey spectra of C1s peak and indicates that the peak intensity of oxygen-containing functional groups such as epoxy/hydroxyl (C-O), carbonyl (C=O), and carboxylate (O-C=O) at 286, 287.2, and 288.1 eV [36, 37] is lower than the C-C peak intensity. This suggests that most of the oxygen-containing functional groups are removed from the surface of GO after electrochemical reduction.

To examine whether present Zn in coating structure is metal or metal oxide, the O1s peak of the XPS spectrum was used (Figure 7(c)). The reported studies [38] demonstrate that, for transition metal oxides such as ZnO, O1s peak is almost placed at 530 eV. Also, the observed O1s peak for ZnO is not single and has two parts that the main part of it results from O_2^- anions in the metal oxide structure. Moreover, the second part of the peak around 531.6 eV has an intensity equivalent to 20% of the intensity of main part. Thus, according to Figure 7(c), which O1s peak of the coating is perfectly symmetrical and single component at 532 ev, we can conclude that Zn in coating structure is pure metal (is not oxidized).

3.2. Surface and Microstructural Characterization

3.2.1. Electron Microscopy. FE-SEM images of synthesized GO nanosheets are illustrated in Figure 8(a). As observed, GO includes random thin, dense, and wavy nanosheets. Wavy state of nanosheets prevents them from sticking and piling

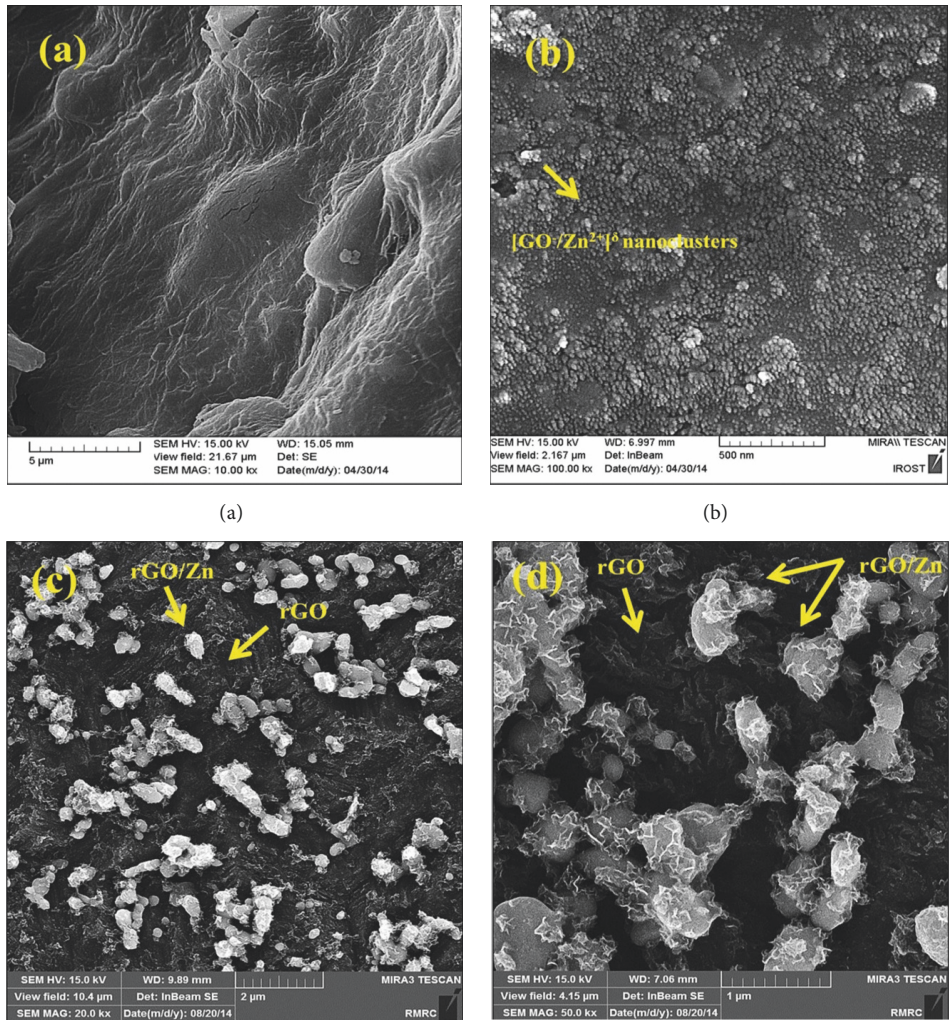

(a) (b)

(c) (d)

Figure 8: FE-SEM images of (a) synthesized GO nanosheets; (b) $[GO^{-}/Zn^{2+}]^{\delta+}$ nanoclusters distributed on GO nanosheets (before pulse-potential electrodeposition); (c) and (d) rGO-Zn coating synthesized by pulse-potential electrodeposition approach.

up [30]. Figure 8(b) shows FE-SEM image of $[GO^{-}/Zn^{2+}]^{\delta+}$ nanoclusters produced by anodic dissolution (before reduction). The average size of clusters is about 25 nm.

But it has been proved that reduced GO layers tend to react with each other and agglomerate to produce a structure with open holes. Also, due to the high specific surface of reduced GO nanosheets, nucleation and growth sites are developed easily on the surface of the sheets [14]. According to Figures 8(c) and 8(d) that show FE-SEM images of rGO-Zn coating, Zn particles are present on reduced graphene oxide sheets and are surrounded by them. Transparency of the sheets indicates that layers are thin and few. The average size of particles is 200 nm.

Figure 9 shows the cross-section FE-SEM images of substrate and coating, used to measure the thickness of rGO-Zn coating (2.3 μm).

3.2.2. AFM Monitoring. Figure 10(a) shows AFM image (edge detection filter mode) of Zn-rGO coating on steel. It is clear that coating is composite and has two phases. It seems that particles are surrounded by thin carbon layers. Topography of the surface is illustrated in Figure 10(b). The amount of Zn nanoparticles plays a key role in the surface roughness of the coating. The height profile (Figure 10(c)) estimates the average surface roughness of about 65 nm. Therefore, coating is relatively rough, indicating that rGO-covered nanoparticles were assembled on the surface.

3.3. Corrosion Behavior Evaluation

3.3.1. Polarization Experiment. To investigate the corrosion behavior of the coatings, potentiodynamic polarization measurements of the rGO-Zn were conducted in a 3.5 wt.% NaCl solution and the results were compared with various surfaces: bare steel, galvanized steel, and steel with rGO coating (Figure 11). The rGO film was deposited on steel through pulse- potential method using the same PED parameters as the rGO-Zn coating.

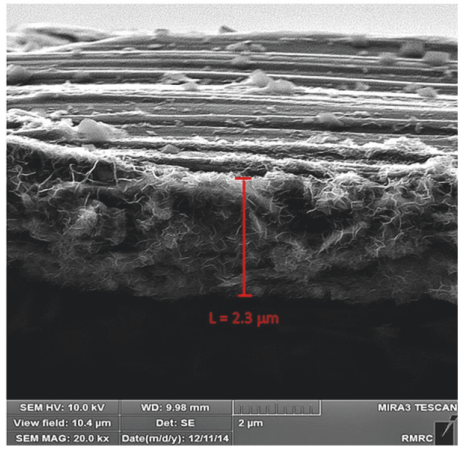

Figure 9: Cross-sectional FE-SEM image of rGO-Zn coating.

In a polarization curve, a higher corrosion potential (E_{Corr} versus SCE) or a lower corrosion current density ($i_{\text{corr.}}$) corresponds to a higher corrosion resistance and lower corrosion rate. Corrosion current density (K) was determined from Tafel plot by extrapolating the linear portion of the curve to E_{corr}. Tafel constants including anodic (βa) and cathodic (βc) slopes were calculated for anodic and cathodic parts of Tafel plot, respectively. Results are summarized in Table 2.

Compared to the bare steel substrate, the corrosion potential of rGO coating changed to less negative values (−0.58 V/SCE to −0.45 V/SCE) [12, 39], but the corrosion resistance is not improved and corrosion current density is increased from 1.5 μA/cm^2 to 1.6 μA/cm^2. While previous studies have demonstrated that graphene layer is corrosion barrier [12, 27, 39] and prevents the contact between substrate and corrosive environment, this result shows that the reduced graphene oxide layer, deposited by pulse-potential method, does probably not cover the entire surface of steel, causing localized corrosion. According to the results in Table 2, corrosion potential of rGO-Zn coating is more negative than bare steel substrate, but less negative in comparison to a zinc-rich coating like galvanized steel, resulting from the simultaneous presence of zinc particles and graphene nanosheets in the coating. Compared to the galvanized steel, the corrosion potential and corrosion current density of the rGO-Zn coating changed from −1.08 V/SCE and 3.0 μA/cm^2 to −0.77 V/SCE and 0.005 μA/cm^2. Given that graphene nanosheets are barrier layers (decrease the corrosion current density and make the corrosion potential less negative) and zinc is the sacrificial anode (increase the corrosion current density and make the corrosion potential more negative), it is observed that however the corrosion potential of rGO-Zn coating changed from −0.58 V to −0.77 V compared to bare steel (more negative value) and the corrosion current density decreased from 1.5 μA/cm^2 to 0.007 μA/cm^2. The corrosion rate (CR) and corrosion inhibition efficiency (η_p) were calculated to analyze the anticorrosion performance of the coatings quantitatively. The CR was estimated using the following formula documented in ASTM standard G10 [40–42]:

$$\text{CR} = \frac{KM_m i_{\text{corr.}}}{\rho_m}, \tag{2}$$

where K is a constant (3268.6 mol/A), M is the molecular weight (56 g/mol), $i_{\text{corr.}}$ is current density (A/cm^2), and ρ_m is the density (7.85 g/cm^3). The CR values of bare steel and steel with rGO/Zn coating were calculated to be 0.035 mm/year and 1.6×10^{-4} mm/year, respectively.

The corresponding corrosion inhibition efficiency (η_p) is calculated by the following equation [43]:

$$\eta_p\,(\%) = \frac{i_{\text{Corr.}}^{\ 0} - i_{\text{Corr.}}}{i_{\text{Corr.}}^{\ 0}} \times 100, \tag{3}$$

where $i_{\text{Corr.}}^{\ 0}$ and $i_{\text{Corr.}}$ are the corrosion current densities without and with the rGO-Zn coating, respectively.

The very low CR and high η_p (99.45%) of the rGO-Zn coating could confirm its superior corrosion resistance due to the combined effect of reduced graphene oxide and zinc. Reduced particle size of zinc can be indicated as another reason for the decrease of corrosion current density in rGO-Zn coating compared to galvanized steel.

3.3.2. EIS. EIS experiments on various steel surfaces were conducted in a 0.1 M KCl solution. Figure 12 shows the Nyquist impedance diagrams of bare steel, galvanized steel, steel with rGO coating (pulse-potential procedure), and steel with rGO-Zn coating.

The Nyquist impedance diagram of the rGO-Zn consists of a depressed semicircle at higher frequencies and big semicircle at low frequency. The depressed semicircle caused by the charge transfer process is related to the charge transfer resistance (R_{ct}) and the double-layer capacitance (C_{dl}) at the graphene layer. Since graphene is a zero gap semiconductor [30], this semicircle is very small and has limited effect on impedance. At lower frequencies, the big semicircle presents coating resistance (R_{Coat}) that implies high corrosion resistance of rGO-Zn coating. The EIS results for bare steel substrate and coated steel can be analyzed with the equivalent circuits shown in Figure 13, and the simulated results are listed in Table 2, where R_s is the electrolyte resistance, C_{dl} is used to denote electrical double-layer capacitance, R_{ct} is the charge transfer resistance, $R_{\text{Coat.}}$ is the resistance of coating, and CPE is the constant phase element of the corrosion layer. The CPE is mathematically expressed as [44]

$$Z_{\text{CPE}} = \frac{1}{Y_0\,(i\omega)^n}, \tag{4}$$

where Y_0 is a proportionality factor and "n" has the meaning of phase shift. The value of "n" represents the deviation from the ideal behavior and it lies between 0 and 1.

The extent of anticorrosive behavior of the coating in corrosive media can be evaluated by EIS plots considering both the coating and charge transfer resistance, that is, the

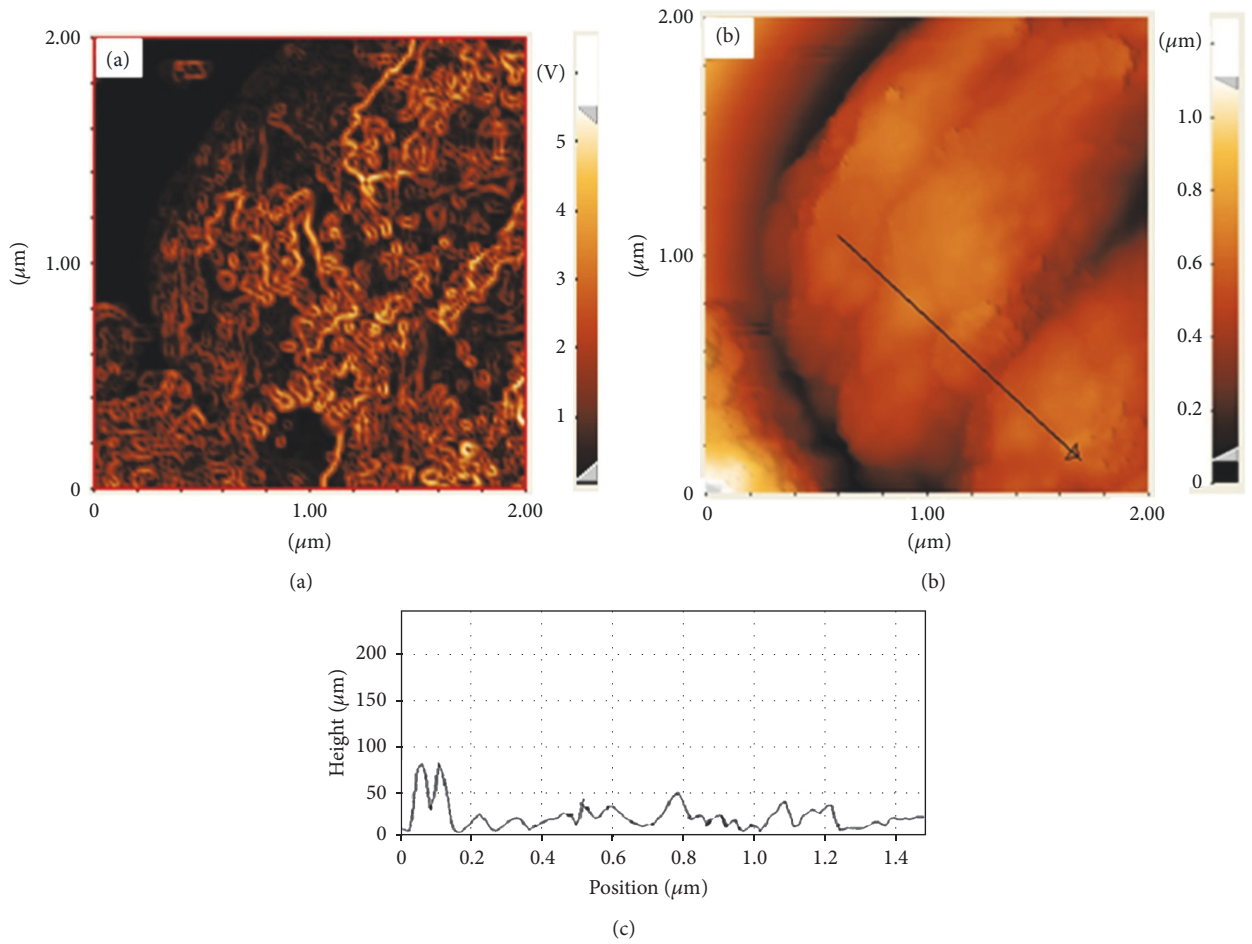

Figure 10: AFM images of rGO-Zn coating produced by pulse-potential electrodeposition approach, (a) edge detection filter mode and (b, c) topography and height profile scanned across the profile line.

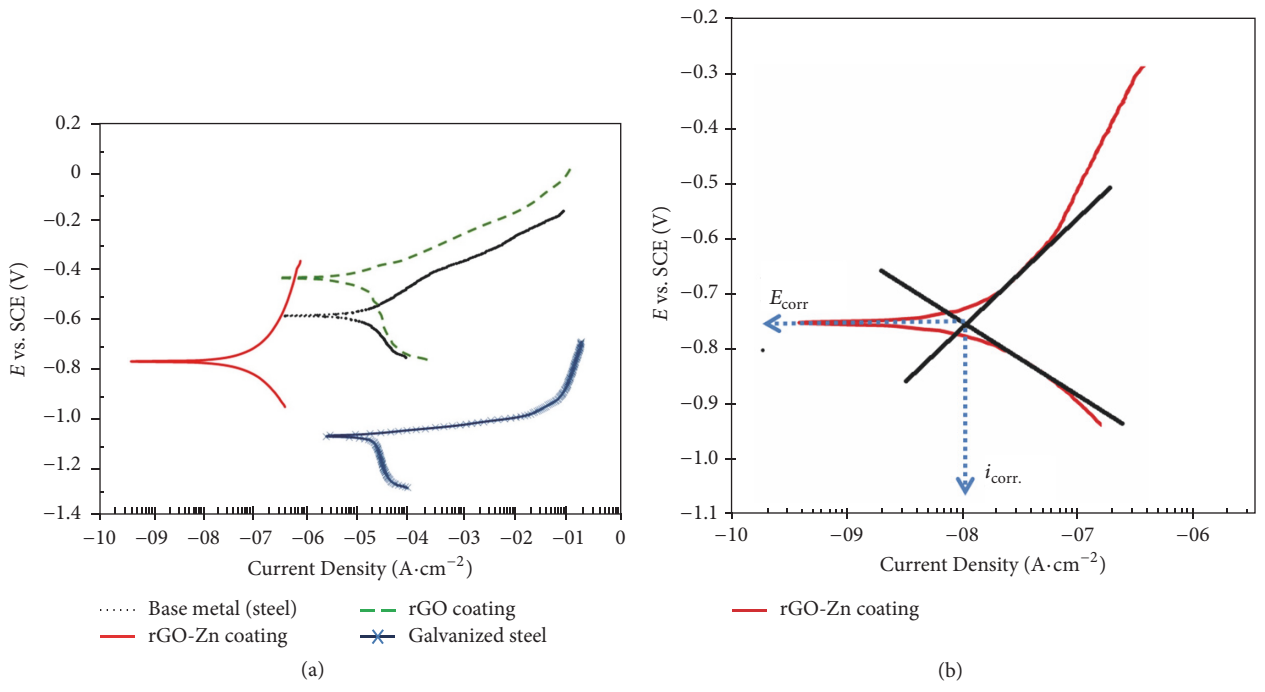

Figure 11: (a) Polarization curves of rGO-Zn coating, bare steel, galvanized steel, and rGO coating after immersion in 3.5 wt.% NaCl solution for 1 h at scan rate 1 mV/s; (b) Tafel extrapolation on the polarization plot of rGO-Zn coating for determination of corrosion current and Tafel slopes.

Table 2: Electrochemical parameters of bare steel, rGO coating, galvanized steel, and rGO-Zn coating; potentiodynamic polarization tests of coatings were accomplished after immersion in 3.5 wt.% NaCl solution for 1 h with scan rate 1 mV/s while EIS tests were achieved at immersing in 0.1 M KCl solution at frequency range of 10^{-3} to 10^{5} Hz with 5 mV ac amplitude and OCP condition (stability time: 30 min).

	Polarization test				EIS test							
Surface	$i_{corr.}$ (μA/cm^2)	$E_{corr.}$ (V/SCE)	$-ß_c$ (mV/decade)	$ß_a$ (mV/decade)	R_s (Ω·cm^2)	CPE$_c$ (μF/cm^2)	n	R_{coat} (Ω·cm^2)	C_{dl} (μF/cm^2)	R_{ct} (Ω·cm^2)	R_p (Ω·cm^2)	CR (mm/year)
Bare steel	1.5	−0.58	34.9	50.6	85.2	79.3	1	-	-	337.6	337.6	0.035
rGO coating	1.6	−0.45	74.5	39.5	85.11	3137	0.82	679.1	431.1	16.02	695.1	0.037
Galvanized steel	3.0	−1.08	21.5	39.7	85.03	30.2	0.68	602.5	570.5	697	1299.5	0.07
rGO-Zn coating	0.007	−0.77	47.0	47.2	90.73	225.4	0.75	3359	23.7	37.63	3396.6	1.6×10^{-4}

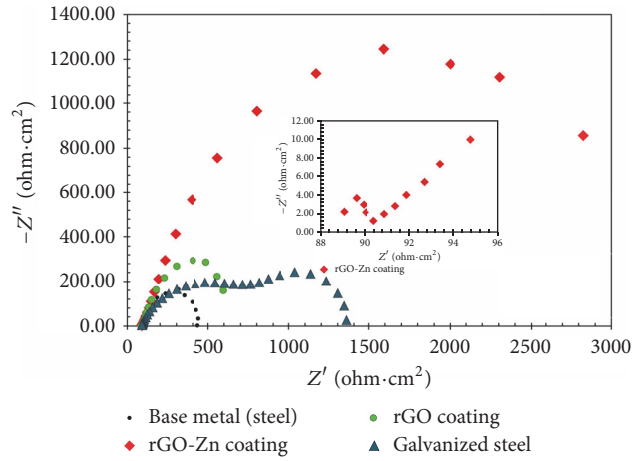

Figure 12: Nyquist plots of rGO-Zn coating, bare steel, galvanized steel, and rGO coating immersed in 0.1 M KCl solution at frequency range of 10^{-3} to 10^{5} Hz with 5 mV ac amplitude and OCP condition (stability time: 30 min).

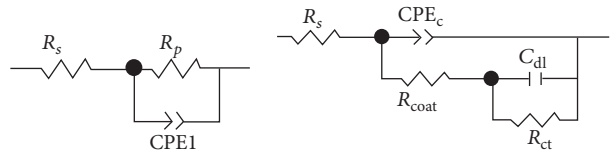

Figure 13: Proposed equivalent circuits for (a) bare steel, (b) galvanized steel, rGO film, and rGO-Zn coating for numerical simulation of the EIS measurements.

polarization resistance (R_p) which is the sum of R_{coat} and R_{ct} (i.e., $R_p = R_{coat} + R_{ct}$) [8, 45]. So, polarization resistance of steel with rGO/Zn coating (3396.63 Ω·cm^2) is about ten times of bare steel (337.6 Ω·cm^2).

4. Conclusion

rGO-Zn nanocomposite coating was successfully fabricated on steel by pulse-potential coelectrodeposition from aqueous suspension of $[GO^-/Zn^{2+}]^{\delta+}$ nanoclusters. FE-SEM observations, as well as all of the XRD, FT-IR, Raman spectroscopy, and XPS results, demonstrated conversion of sp^3 structure to sp^2 domains and removal of most oxygen-containing functional groups from the surface of GO nanosheets after electrochemical pulse reduction and showed the formation of zinc metal particles (<200 nm) in the nanocomposite coating. AFM represented that nanocomposite film was relatively rough with the average surface roughness of about 65 nm due to rGO-covered zinc nanoparticles on the surface. Regarding the corrosion behavior of steel, not only was polarization resistance of the substrate increased about ten times after the rGO/Zn nanocomposite coating was applied, but also corrosion rate was decreased from 0.034 mm/year to 1.62 × 10^{-4} mm/year. This was represented the synergistic effect of reduced graphene oxide as a barrier layer as well as zinc element as a sacrificial anode in the coating.

Conflicts of Interest

The authors declare that there are no conflicts of interest regarding the publication of this paper.

References

[1] C. M. P. Kumar, T. V. Venkatesha, and R. Shabadi, "Preparation and corrosion behavior of Ni and Ni-graphene composite coatings," *Materials Research Bulletin*, vol. 48, no. 4, pp. 1477–1483, 2013.

[2] K. M. S. Youssef, C. C. Koch, and P. S. Fedkiw, "Improved corrosion behavior of nanocrystalline zinc produced by pulse-current electrodeposition," *Corrosion Science*, vol. 46, no. 1, pp. 51–64, 2004.

[3] M. Mouanga, L. Ricq, J. Douglade, and P. Berçot, "Corrosion behaviour of zinc deposits obtained under pulse current electrodeposition: Effects of coumarin as additive," *Corrosion Science*, vol. 51, no. 3, pp. 690–698, 2009.

[4] M. S. Chandrasekar, Shanmugasigamani, and P. Malathy, "Synergetic effects of pulse constraints and additives in electrodeposition of nanocrystalline zinc: Corrosion, structural and textural characterization," *Materials Chemistry and Physics*, vol. 124, no. 1, pp. 516–528, 2010.

[5] H. B. Muralidhara and Y. Arthoba Naik, "Electrochemical deposition of nanocrystalline zinc on steel substrate from acid zincate bath," *Surface and Coatings Technology*, vol. 202, no. 14, pp. 3403–3412, 2008.

[6] K. Schaefer and A. Miszczyk, "Improvement of electrochemical action of zinc-rich paints by addition of nanoparticulate zinc," *Corrosion Science*, vol. 66, pp. 380–391, 2013.

[7] R. Ramanauskas, L. Gudavičiute, R. Juškenas, and O. Ščit, "Structural and corrosion characterization of pulse plated nanocrystalline zinc coatings," *Electrochimica Acta*, vol. 53, no. 4, pp. 1801–1810, 2007.

[8] M. K. Punith Kumar, M. P. Singh, and C. Srivastava, "Electrochemical behavior of Zn-graphene composite coatings," *RSC Advances*, vol. 5, no. 32, pp. 25603–25608, 2015.

[9] R. V. Dennis, L. T. Viyannalage, A. V. Gaikwad, T. K. Rout, and S. Banerjee, "Graphene nanocomposite coatings for protecting low-alloy steels from corrosion," *American Ceramic Society Bulletin*, vol. 92, pp. 18–24, 2013.

[10] N. T. Kirkland, T. Schiller, N. Medhekar, and N. Birbilis, "Exploring graphene as a corrosion protection barrier," *Corrosion Science*, vol. 56, pp. 1–4, 2012.

[11] B. P. Singh, S. Nayak, K. K. Nanda, B. K. Jena, S. Bhattacharjee, and L. Besra, "The production of a corrosion resistant graphene reinforced composite coating on copper by electrophoretic deposition," *Carbon*, vol. 61, pp. 47–56, 2013.

[12] E. T. Lih, R. B. Zaid, L. L. Tan, and K. F. Chong, "Facile Corrosion Protection Coating from Graphene," *International Journal of Chemical Engineering and Applications*, pp. 453–455, 2012.

[13] M. Hilder, O. Winther-Jensen, B. Winther-Jensen, and D. R. MacFarlane, "Graphene/zinc nano-composites by electrochemical co-deposition," *Physical Chemistry Chemical Physics*, vol. 14, no. 40, pp. 14034–14040, 2012.

[14] W. He, L. Zhu, H. Nan, H. Liu, and W. Li, "Thin Film of Zn/rGO Nanocomposites Fabricated by Electrodeposition," *International Journal of Materials Science and Engineering*, pp. 32–35, 2013.

[15] W. S. Hummers Jr. and R. E. Offeman, "Preparation of graphitic oxide," *Journal of the American Chemical Society*, vol. 80, no. 6, p. 1339, 1958.

[16] Y. Yaghoubinezhad and A. Afshar, "Experimental design for optimizing the corrosion resistance of pulse reverse electrodeposited graphene oxide thin film," *Journal of Solid State Electrochemistry*, vol. 19, no. 5, pp. 1367–1380, 2015.

[17] A. I. Yanson, P. Rodriguez, N. Garcia-Araez, R. V. Mom, F. D. Tichelaar, and M. T. M. Koper, "Cathodic corrosion: A quick, clean, and versatile method for the synthesis of metallic nanoparticles," *Angewandte Chemie International Edition*, vol. 50, no. 28, pp. 6346–6350, 2011.

[18] H. Wang, X. Yuan, Y. Wu et al., "Adsorption characteristics and behaviors of graphene oxide for Zn (II) removal from aqueous solution," *Applied Surface Science*, vol. 279, pp. 432–440, 2013.

[19] W. Ye, X. Zhang, Y. Chen, Y. Du, F. Zhou, and C. Wang, "Pulsed electrodeposition of reduced graphene oxide on glass carbon electrode as an effective support of electrodeposited Pt microspherical particles: nucleation studies and the application for methanol electro-oxidation," *International Journal of Electrochemical Science*, vol. 8, pp. 2122–2139, 2013.

[20] M. S. Chandrasekar and M. Pushpavanam, "Pulse and pulse reverse plating-conceptual, advantages and applications," *Electrochimica Acta*, vol. 53, no. 8, pp. 3313–3322, 2008.

[21] J. Wu, X. Shen, L. Jiang, K. Wang, and K. Chen, "Solvothermal synthesis and characterization of sandwich-like graphene/ZnO nanocomposites," *Applied Surface Science*, vol. 256, no. 9, pp. 2826–2830, 2010.

[22] G. Du, X. Wang, L. Zhang, Y. Feng, and Y. Liu, "One-step green synthesis of graphene-ZnO nanocomposites," *Materials Letters*, vol. 98, pp. 168–170, 2013.

[23] G. Du, X. Wang, L. Zhang, Y. Feng, and Y. Li, "Controllable synthesis of different ZnO architectures decorated reduced graphene oxidenanocomposites," *Materials Letters*, vol. 96, pp. 128–130, 2013.

[24] S. Pourhashem, M. R. Vaezi, A. Rashidi, and M. R. Bagherzadeh, "Exploring corrosion protection properties of solvent based epoxy-graphene oxide nanocomposite coatings on mild steel," *Corrosion Science*, vol. 115, pp. 78–92, 2017.

[25] T. Lu, Y. Zhang, H. Li, L. Pan, Y. Li, and Z. Sun, "Electrochemical behaviors of graphene-ZnO and graphene-SnO_2 composite films for supercapacitors," *Electrochimica Acta*, vol. 55, no. 13, pp. 4170–4173, 2010.

[26] S. Pan and X. Liu, "ZnS-Graphene nanocomposite: Synthesis, characterization and optical properties," *Journal of Solid State Chemistry*, vol. 191, pp. 51–56, 2012.

[27] T. Rattana, S. Chaiyakun, N. Witit-Anun et al., "Preparation and characterization of graphene oxide nanosheets," *Procedia Engineering*, vol. 32, pp. 759–764, 2012.

[28] G. K. Ramesha and N. S. Sampath, "Electrochemical reduction of oriented Graphene oxide films: An in situ Raman spectroelectrochemical study," *The Journal of Physical Chemistry C*, vol. 113, no. 19, pp. 7985–7989, 2009.

[29] P. She, S. Yin, Q. He et al., "A self-standing macroporous Au/ZnO/reduced graphene oxide foam for recyclable photocatalysis and photocurrent generation," *Electrochimica Acta*, vol. 246, pp. 35–42, 2017.

[30] V. Singh, D. Joung, L. Zhai, S. Das, S. I. Khondaker, and S. Seal, "Graphene based materials: past, present and future," *Progress in Materials Science*, vol. 56, no. 8, pp. 1178–1271, 2011.

[31] Z. Ni, Y. Wang, T. Yu, and Z. Shen, "Raman spectroscopy and imaging of graphene," *Nano Research*, vol. 1, no. 4, pp. 273–291, 2008.

[32] G. Sobon, J. Sotor, J. Jagiello et al., "Graphene Oxide vs. Reduced Graphene Oxide as saturable absorbers for Er-doped passively mode-locked fiber laser," *Optics Express*, vol. 20, no. 17, pp. 19463–19473, 2012.

[33] S. Stankovich, D. A. Dikin, R. D. Piner et al., "Synthesis of graphene-based nanosheets via chemical reduction of exfoliated graphite oxide," *Carbon*, vol. 45, no. 7, pp. 1558–1565, 2007.

[34] A. S. Kousalya, A. Kumar, R. Paul, D. Zemlyanov, and T. S. Fisher, "Graphene: An effective oxidation barrier coating for liquid and two-phase cooling systems," *Corrosion Science*, vol. 69, pp. 5–10, 2013.

[35] X.-Y. Peng, X.-X. Liu, D. Diamond, and K. T. Lau, "Synthesis of electrochemically-reduced graphene oxide film with controllable size and thickness and its use in supercapacitor," *Carbon*, vol. 49, no. 11, pp. 3488–3496, 2011.

[36] D. C. Marcano, D. V. Kosynkin, J. M. Berlin et al., "Improved synthesis of graphene oxide," *ACS Nano*, vol. 4, no. 8, pp. 4806–4814, 2010.

[37] L. Tang, Y. Wang, Y. Li, H. Feng, J. Lu, and J. Li, "Preparation, structure, and electrochemical properties of reduced graphene sheet films," *Advanced Functional Materials*, vol. 19, no. 17, pp. 2782–2789, 2009.

[38] J.-C. Dupin, D. Gonbeau, P. Vinatier, and A. Levasseur, "Systematic XPS studies of metal oxides, hydroxides and peroxides," *Physical Chemistry Chemical Physics*, vol. 2, no. 6, pp. 1319–1324, 2000.

[39] S. Chen, L. Brown, M. Levendorf et al., "Oxidation resistance of graphene-coated Cu and Cu/Ni alloy," https://arxiv.org/abs/1011.3875.

[40] X. Sheng, W. Cai, L. Zhong, D. Xie, and X. Zhang, "Synthesis of Functionalized Graphene/Polyaniline Nanocomposites with Effective Synergistic Reinforcement on Anticorrosion," *Industrial & Engineering Chemistry Research*, vol. 55, no. 31, pp. 8576–8585, 2016.

[41] C.-H. Chang, T.-C. Huang, C.-W. Peng et al., "Novel anticorrosion coatings prepared from polyaniline/graphene composites," *Carbon*, vol. 50, no. 14, pp. 5044–5051, 2012.

[42] S. C. Sahu, A. K. Samantara, M. Seth et al., "A facile electrochemical approach for development of highly corrosion protective coatings using graphene nanosheets," *Electrochemistry Communications*, vol. 32, pp. 22–26, 2013.

[43] M. A. Migahed, E. M. S. Azzam, and A. M. Al-Sabagh, "Corrosion inhibition of mild steel in 1 M sulfuric acid solution using anionic surfactant," *Materials Chemistry and Physics*, vol. 85, no. 2-3, pp. 273–279, 2004.

[44] P. Mourya, S. Banerjee, and M. M. Singh, "Corrosion inhibition of mild steel in acidic solution by *Tagetes erecta* (Marigold flower) extract as a green inhibitor," *Corrosion Science*, vol. 85, pp. 352–363, 2014.

[45] K. Deepa, T. V. Venkatesha, C. Nagaraja, and M. R. Vinutha, "Electrochemical Corrosion Studies of Zn-CuO and Zn-NiO-CuO Composite Coatings on Mild Steel," *Analytical and Bioanalytical Electrochemistry*, vol. 9, no. 3, pp. 374–389, 2017.